# Observations of the Antarctic Slope Current in the Southeastern Weddell Sea: A Bottom-Enhanced Current and Its Seasonal Variability

Elin Darelius, I. Fer, M. Janout, K. Daae, Nadine Steiger

JGR Oceans

RESEARCH ARTICLE
10.1029/2023JC020666

# Observations of the Antarctic Slope Current in the Southeastern Weddell Sea: A Bottom-Enhanced Current and Its Seasonal Variability

**E. Darelius[1], I. Fer[1], M. Janout[2], K. Daae[1], and N. Steiger[3]**

[1]Geophysical Institute, University of Bergen and the Bjerknes Centre for Climate Research, Bergen, Norway, [2]Alfred-Wegener-Institute Helmholtz Center for Polar and Marine Research, Bremerhaven, Germany, [3]Sorbonne Université, CNRS/IRD/MNHN, LOCEAN-IPSL, Paris, France

**Key Points:**

- Four years of observations show that the Antarctic Slope Current north of the Filchner Trough is bottom-enhanced and strongest during winter
- The bottom enhancement is linked to isotherms that slope upward toward the shelf break, facilitating on-shelf transport of warm water
- On monthly to seasonal time scales, positive temperature anomalies above the slope are associated with weaker-than-normal currents and vice versa

**Correspondence to:**
E. Darelius,
elin.darelius@uib.no

**Citation:**
Darelius, E., Fer, I., Janout, M., Daae, K., & Steiger, N. (2024). Observations of the Antarctic slope current in the southeastern Weddell Sea: A bottom-enhanced current and its seasonal variability. *Journal of Geophysical Research: Oceans*, *129*, e2023JC020666. https://doi.org/10.1029/2023JC020666

Received 3 NOV 2023
Accepted 28 MAY 2024

**Author Contributions:**
**Conceptualization:** E. Darelius
**Data curation:** E. Darelius
**Formal analysis:** E. Darelius, K. Daae
**Funding acquisition:** E. Darelius
**Methodology:** E. Darelius, I. Fer, K. Daae
**Project administration:** E. Darelius
**Resources:** E. Darelius, I. Fer, M. Janout, N. Steiger
**Visualization:** K. Daae
**Writing – original draft:** E. Darelius
**Writing – review & editing:** I. Fer, M. Janout, K. Daae, N. Steiger



**Abstract** The Antarctic Slope Front and the associated Antarctic Slope Current dynamically regulate the exchanges of heat across the continental shelf break around Antarctica. Where the front is weak, relatively warm deep waters reach the ice shelf cavities, contributing to basal melting and ultimately affecting sea level rise. Here, we present new 2017–2021 records from two moorings deployed on the upper continental slope (530 and 738 m depth) just upstream of the Filchner Trough in the southeastern Weddell Sea. The structure and seasonal variability of the frontal system in this region, central to the inflow of warm water toward the large Filchner-Ronne Ice Shelf, is previously undescribed. We use the records to describe the mean state and the seasonal variability of the regional hydrography and the southern part of the Antarctic Slope Current. We find that (a) the current is, contrary to previous assumptions, bottom-enhanced, (b) the isotherms slope upwards toward the shelf break, and more so for warmer isotherms, and (c) the monthly mean thermocline depth is shallowest in February-March and deepest in May-June while (d) the current is strongest in April-June. On monthly timescales, we show that (e) positive temperature anomalies of the de-seasoned records are associated with weaker-than-average currents. We propose that the upward-sloping isotherms are linked to the local topography and conservation of potential vorticity. Our results contribute to the understanding of how warm ocean waters propagate southward and potentially affect basal melt rates at the Filchner-Ronne Ice Shelf.

**Plain Language Summary** Melting at the base of the Filchner-Ronne Ice Shelf in the southeastern Weddell Sea is predicted to increase dramatically. The melt occurs within the ice shelf cavity filled with seawater, and the heat needed to melt the ice comes from warm water from the deep ocean. The warm water is carried toward the cavities over the relatively shallow continental shelves by ocean currents. The Antarctic Slope Current, a current that flows along the continental slope between cold and warm water masses, limits the amount of warm water that enters the continental shelf. Here, we use new four year-long mooring records from the upper part of the continental slope north of the Filchner-Ronne Ice Shelf and just east of the Filchner Trough to describe how the current changes with the season and how its vertical structure evolves throughout the year. We find that the warm water is lifted up toward the shelf break and suggest that this is linked to the presence of the Filchner Trough. An improved understanding of the dynamics of the Antarctic Slope Current in the region will allow us to better evaluate the potential for dramatic changes to the system in the future.

## 1. Introduction

The Antarctic Slope Front (ASF) is a thermohaline front that separates the cold waters on the shallow continental shelf from the comparatively warm Circumpolar Deep Water (CDW) found at depth off the continental shelf (Orsi et al., 2002; Whitworth et al., 1998). The ASF is formed as prevailing easterly winds and southward surface Ekman transport cause surface water to converge along the coast, elevating the sea surface along the Antarctic coastline and depressing the isopycnals (Sverdrup, 1953). Topographic potential vorticity constraints and buoyancy forcing also contribute to the formation of the ASF (Thompson et al., 2018, 2020). The ASF dynamically supports the Antarctic Slope Current (ASC; Jacobs, 1986), which flows westward around most of the Antarctic continent. The meridional slope of the front, together with tides and eddies (Stewart et al., 2019), regulates the strength of the ASC and the accessibility of the CDW to the continental shelf. A relaxed, relatively flat ASF means that CDW is higher up in the water column and more likely to enter the shelf. The dynamics of the ASF/ASC system thus largely determine the on-shelf oceanic heat flux and, ultimately, the amount of heat

reaching the cavities beneath the ice shelves fringing the Antarctic Ice Sheet (Heywood et al., 2014). In regions where the slope of the ASF is gentle, for example, in the Amundsen Sea, the continental shelves and the ice shelf cavities are flooded with CDW, and basal melt rates are high (e.g., Pritchard et al., 2012; Rignot et al., 2013; Shepherd et al., 2018). The steeper ASF in the Weddell Sea, on the other hand, causes the thermocline to incrop at the continental slope below the depth of the shelf break. In this region, the thermocline marks the interface between the Warm Deep Water (WDW), the slightly cooler and fresher version of CDW specific to the Weddell Sea, and the colder Winter Water (WW) above. The WDW and the modified WDW (mWDW), which is a mixture of WDW and WW, hence has limited access to the Weddell shelf but is channeled southward along the flanks of Filchner Trough (Darelius et al., 2016; Ryan et al., 2017, see Figure 1 for location) and the Central Trough west of the Berkner Bank (at 44°W, Nicholls et al., 2008). The WDW inflow occurs particularly during summer when the ASF relaxes, and WDW reaches higher up in the water column (Semper & Darelius, 2017; Årthun et al., 2012).

The waters of the wide continental shelf and the Filchner-Ronne Ice Shelf (FRIS) cavity are, in general, characterized by temperatures close to or below the surface freezing point (Nicholls et al., 2009), resulting in relatively low melt rates beneath FRIS. Future projections suggest a potential regime shift in the southern Weddell Sea, with WDW flooding the continental shelf and a dramatic increase in basal melt rates beneath FRIS. The shift is predicted to occur within this century (Hellmer et al., 2012, 2017) or possibly beyond 2100 (Naughten et al., 2021; Nissen et al., 2022), and it would require a combination of changes in the thermocline depth over the continental slope and a reduction in the density of the cold and dense Ice Shelf Water (ISW). The latter currently prevents WDW from accessing Filchner Trough and the FRIS cavity (Daae et al., 2020). The impact of increased melting beneath FRIS on the acceleration and thinning of the upstream ice sheet and the global sea level rise is debated (Hill et al., 2021), as observations poorly constrain the models used for these predictions. Paleo-records and simulations, however, identify the southern Weddell Sea and the Recovery basin as a region sensitive to change (Stokes et al., 2022). To better predict the likelihood and timing of a regime shift at FRIS, we must understand the dynamics controlling the ASF/ASC system and the flow of WDW across the shelf break in the southeastern Weddell Sea.

Previous observations of the westward-flowing ASC in the Weddell Sea have mostly been obtained from the "fresh shelf domain" in the eastern Weddell Sea (Thompson et al., 2018). Here, the continental shelf is narrow and characterized by cold and fresh waters, and the ASC/ASF is near the ice fronts. In this area, the ASC is merged with the coastal current, which follows the coastline and ice fronts around Antarctica (Heywood et al., 1998). The ASC is surface-intensified (Chavanne et al., 2010; Heywood et al., 1998) with annual mean core velocities off Kapp Norwegian ranging from 10 to 20 cm/s (Fahrbach et al., 1992, see Figure 1 for location). It displays a relatively strong seasonal variation, reaching its maximum strength in the autumn (Fahrbach et al., 1992; Nunez-Riboni & Fahrbach, 2009). This seasonal pattern appears coherent along the southern rim of the Weddell Sea (Le Paih et al., 2020). The surface-intensified, westward current weakens with increasing depth as the isopycnals slope downwards toward the south. In the eastern Weddell Sea (0–17°W), an eastward undercurrent at deeper levels has been observed (Chavanne et al., 2010; Heywood et al., 1998; Nunez-Riboni & Fahrbach, 2009), where the steep southward isopycnal slope forces baroclinic eastward flow that dominates the westward, barotropic component. Toward the sea floor, however, the tilt of the isopycnals here often reverses, that is, the isopycnals shoal toward the coast, potentially due to bottom Ekman transport (Smedsrud et al., 2006) and/or eddy overturning (Hattermann et al., 2014; Nøst et al., 2011; Stewart & Thompson, 2015).

The ASC separates from the coast and the coastal current near 27°W (Foster & Carmack, 1976), where the continental shelf widens. In this region, relatively dense water masses on the continental shelf give rise to a V-shaped pycnocline co-located with the shelf break (Gill, 1973), marking a transition into a "dense shelf domain" (Thompson et al., 2018). Consequently, descriptions of ASC properties and variability based on observations from the "fresh domain" east of 27°W do not directly apply to the transition region around Filchner Trough – a region identified as central for the inflow of WDW (Hellmer et al., 2012; Ryan et al., 2017), the outflow of dense ISW, and the formation of Antarctic Bottom Water (Foldvik et al., 2004). An unprecedented warming of the WDW core above the upper continental slope has been observed in 2021, accompanied by a freshening of the overlying WW to the north of Filchner Trough (Darelius et al., 2023). Although this warming does not appear to have propagated onto the continental shelf, where the inflow was warmer and stronger in 2017–2018 (Ryan et al., 2020), it highlights the need to improve our understanding of the dynamics and variability of the ASC/ASF system in the Filchner Trough region. A comprehensive, observation-based description of the structure of the ASC/ASF system in this region is, however, lacking.

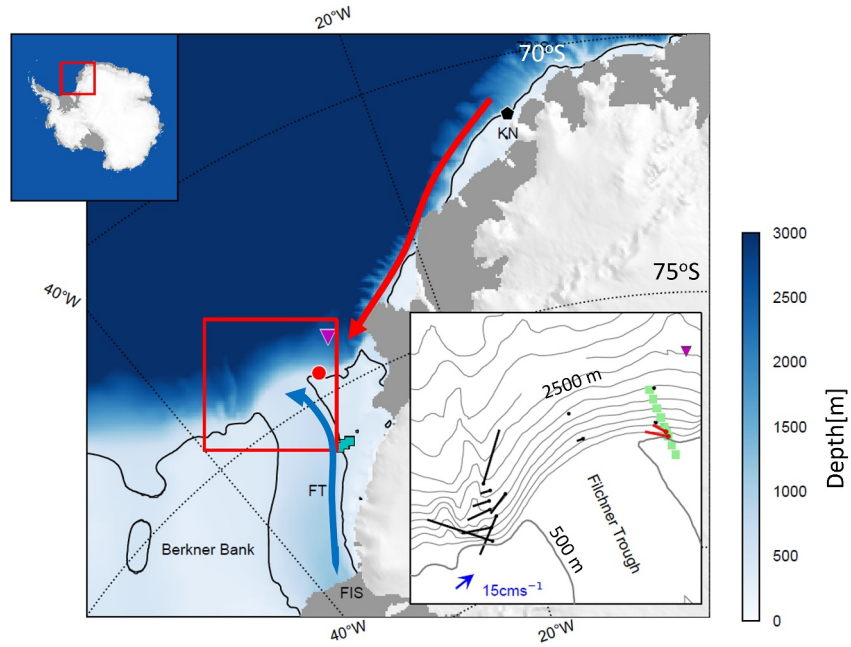


**Figure 1.** Map over the study area with bathymetry (Fretwell et al., 2013) in blue shading according to the colorbar. The 500 m isobath is highlighted in black. The circulation in the area is shown with blue (outflow of ISW) and red (slope front and coastal current) arrows (Darelius et al., 2014; Ryan et al., 2017), and the positions of the $M_{530/740}$ (red circle), $M_{2570}$ (magenta triangle), Kapp Norwegian (black pentagon) moorings and continental shelf (CS) moorings at 76°S (cyan squares) are indicated. Floating ice shelves are shown in dark gray and land in light gray. FT indicates Filchner Trough, KN is Kapp Norwegian, and FIS is the Filchner Ice Shelf. The insets show (upper, left) the position of the study area and (lower, right) a zoom-in to the area marked with a red rectangle in the main figure, covering the upper part of the continental slope at Filchner Trough opening. In the latter, positions of the CTD-section shown in Figure 2 are marked with green squares and mean currents (25 mab) from historical moorings (black dots, Daae et al., 2017; Foldvik et al., 2004; Jensen et al., 2013) and $M_{740}$ and $M_{530}$ (red dots) are shown as black and red sticks, respectively. The blue arrow on the continental shelf in the lower left corner gives the velocity scale. Isobaths are shown every 250 m, with the 500 m isobath in bold.

In this study, we contribute to filling this gap by describing the mean properties and the seasonality of the ASC/ASF and the hydrography on the upper continental slope east of the Filchner Trough. Our analysis is based on a dataset spanning four years, from 2017 to 2021, obtained from oceanographic moorings deployed at depths of 530, 740, and 2570 m. We make use of (a) two neighboring continental slope moorings to quantify the slope of the isotherms/isopycnals in the vicinity of the shelf break and (b) the length of the records to describe the average seasonal patterns and to identify links between the strength of the ASC and temperature anomalies on monthly to seasonal time scales. We use hydrographic data from ships and instrumented Weddell Seals to discuss the broader context.

## 2. Data and Methods

### 2.1. Mooring Data

We present results from three oceanographic moorings, operated on the continental slope east of Filchner Trough (Figure 1) from 2017 to 2021. The moorings were deployed and recovered during the WAPITI (JCR16004, Sallée, 2017) and COSMUS (PS124 Hellmer & Holtappels, 2021) expeditions in February 2017 and 2021, respectively. Two moorings were deployed on the upper continental slope: $M_{740}$ (74°33.00' S, 29°54.48' W) at 740 m depth and $M_{530}$ (74°35.70' S, 29°54.97' W) at 530 m depth. These moorings were equipped with current meters: 75 kHz (2 hr) and 150 kHz (1 hr) Acoustic Doppler Current Profilers from RDI, Recording Current Meters from Aanderaa (2 hr), and hydrographic sensors: SBE37 (600 s), SBE39 (900 s), and SBE56 (120 s) from Seabird Electronics (SBE), where the number in parenthesis gives the maximum sampling interval used for that instrument type (see Table 1 and Figure 2). The third mooring, $M_{2570}$ (74° 1.17' S, 28° 4.78' W) at 2750 m depth, was deployed to hold a sound source (for Argo positioning), but also included two temperature sensors (one SBE39

**Table 1**
*Details About Moorings and Mooring Instrumentation*

| | Position | Period | Bottom depth [m] | Depth of hydrography sensors [m] | Depth of velocity bins [m] |
|---|---|---|---|---|---|
| $M_{530}$ | 74°35.70' S, 29°54.97' W | 2017–2021 | 530 | 505, **496**, 471, 456, **431**, 404, 379, **354**, 328 | 26:8:298, 506[a] |
| $M_{740}$ | 74°33.00' S, 29°54.48' W | 2017–2021 | 740 | 716, **707**, 682, 657, 632, **604**, 579, 554, **529**, 503, 478, 453, 428, 403, 378, 353, **328**, 303 | 46:16:478, 717[a] |
| $M_{2570}$ | 74° 1.17' S, 28° 4.78' W | 2017–2021 | 2570 | 571, 371 | |
| CS | ~76°S 30.5/31°S | 2014–2021 | ~450 | **430**, **330** | 430[a] |

*Note.* Depths with sensors for temperature and salinity are given in bold, and depths with only temperature are given in normal font. Ranges for velocity measurements with ADCP are given as shallowest bin: bin size: deepest bin. [a]Point measurement.

and one SBE56, Table 1). Additionally, one year-long records from a mooring deployed at approximately the same position as $M_{740}$ in 2009 (Jensen et al., 2013) complement the study.

The data from $M_{740}$ and $M_{530}$ were processed as described in Darelius (2023). If not stated otherwise, analyses are performed using hourly averaged values (bi-hourly records are interpolated linearly). Where low-pass filtered data are shown, a fifth-order Butterworth filter with a cut-off period of 48 hr was applied. The alongslope current is obtained by rotating the coordinate system 146° counterclockwise, which roughly aligns the $x$-axis with the time-averaged current at 300 m above bottom (mab). Moorings $M_{530}$ and $M_{740}$ are separated by 5 km, and $M_{2570}$ is located 80 km from $M_{740}$. An integral timescale was estimated following Emery and Thomson (2001), giving values around or below seven days (a week) for the velocity records. The effective degrees of freedom (DOF) can then be estimated by the number of observations divided by the number of hours in a week and the standard error by the standard deviation divided by the square root of DOF.

For comparison, data from moorings deployed between 2014 and 2021 at 76°S on the continental shelf east of Filchner Trough (CS, Ryan et al., 2017, cyan squares in Figure 1) are discussed in the text.

### 2.2. Auxiliary Data

CTD (conductivity-temperature-depth) profiles from the continental slope are available from the deployment cruise in 2017 (Sallée, 2017) and the recovery cruise in 2021 (Hellmer & Holtappels, 2021). The position of the CTD profiles included in the study is shown in Figure 1.

In addition, we use CTD profiles collected by instrumented Weddell Seals (downloaded from MEOP, Treasure et al., 2017). Profiles from the study area are available from 2007 (Nicholls et al., 2008, 2009), 2011 (Årthun et al., 2012), and 2014 (Nachtsheim et al., 2019). We include 112 profiles from the continental slope area upstream of Filchner Trough (30°45' W–25°30' W), where the temperature indicates a thick WW layer ($\Theta < -1.8$°C at 150 m depth). The profiles are binned according to month (February, April, June) and isobaths (500–600 m and 600–700 m). The number of profiles varies with year and month, with a total of 30 profiles from February (21 from 2007 to nine from 2009), 43 profiles from April (16 from 2007, 25 from 2011, to two from 2014), and 39 profiles from June (8 from 2007 to 31 from 2011).

Mooring records are compared to results extracted from a gridded monthly mean climatology compiled by Hattermann (2018), based on data from the region around Kapp Norwegian (see Figure 1 for location).

Monthly mean sea ice concentrations and zonal 10 m-wind velocities are extracted from the ERA5 reanalysis (Hersbach et al., 2020) for the period 1979–2021 and averaged over the region 24–36°W, 73–75.5°S.

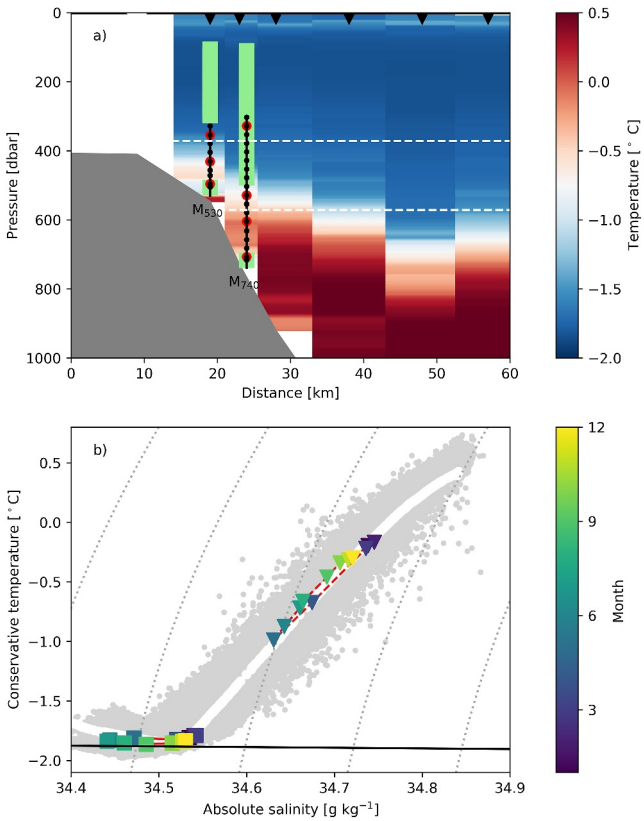


**Figure 2.** (a) Temperature sections across the continental slope at the position of mooring $M_{740}$ and $M_{530}$ (roughly along 30°W, see Figure 1 for location) occupied 25 February (duration 17 hr) in 2017. The position of individual CTD profiles is indicated with black triangles along the upper *x*-axis. The position of the moorings is indicated in (a), where black dots denote temperature sensors, red circles salinity sensors, and where levels with velocity records are marked in green. The dashed white lines show the target depth of the temperature sensors at $M_{2570}$. (b) $\Theta$-$S_A$ diagram showing monthly mean hydrography from $M_{740}$ at 707 m (triangles) and 328 m (squares) depth color-coded with respect to time. The gray dots show the complete hydrography record from the mooring, while the CTD-cast occupied in the vicinity of the mooring site on recovery (February 2021) is shown in white.

### 2.3. Isotherm Slope and the Relation Between Temperature and Density

The slope of the isotherms between the two moorings on the upper continental slope is proportional to the difference in isotherm depth observed at the adjacent moorings:

$$\Delta\mathrm{ITD}(\theta,t) = \mathrm{ITD}(\theta,t)_{\mathrm{M}_{740}} - \mathrm{ITD}(\theta,t)_{\mathrm{M}_{530}} \quad (1)$$

where $\mathrm{ITD}(\theta,t)_{M_X}$ is the depth of the isotherm $\theta$, inferred through linear interpolation (in the vertical, resolution 5 m) at each time step at mooring $M_X$. $\Delta$ITD ($\theta$, $t$) is calculated only when the isotherm was captured in both $M_{740}$ and $M_{530}$.

At the depths covered by $M_{530}$ and $M_{740}$ and within the relevant temperature range (−1.5°C to 0.4°C), the density anomaly referenced to 600 m ($\sigma_{600}$) can be approximated from the Conservative Temperature, $\Theta$, using the CTD data and linear regression as

$$\sigma_{600} = 0.037\Theta + 30.6 \quad (2)$$

Isopycnals are thus parallel to isotherms, and a positive value of $\Delta$ITD represents isotherms and isopycnals that slope upward toward the shelf break.

## 3. Results

### 3.1. Mean Hydrography and Currents

Moorings $M_{530}$ and $M_{740}$ were deployed at the upper continental slope, separated by about 5 km. The upper (above 400 m) water column covered by the moorings is dominated by relatively cold and fresh WW, while the deeper part is (mostly) surrounded by warm mWDW (Figure 2). The moorings, hence, typically capture the thermocline and the upper part of the WDW layer. Tidal currents at this site are relatively strong and seasonally enhanced by resonant shelf waves (Semper & Darelius, 2017). After the tides are filtered out, the current is quasi-unidirectional and directed westward along the slope (Figures 3c and 3d). Variability on shorter time scales, for example, episodic warm inflows forced by wind events or energetic continental shelf waves that vertically displace the thermocline by $\mathcal{O}(100)$ m on daily to weekly time scales (Jensen et al., 2013; Semper & Darelius, 2017) will be discussed elsewhere.

The moorings are located within the southern part of the ASC, and the mean current is directed westward along the isobaths (Figures 1 and 4) with mean velocities of 0.10 m $s^{-1}$. The upper instruments (above 350 m) of the moorings are surrounded by cold ($\Theta \simeq -1.9$°C) water, and the time-averaged temperatures at each mooring increase monotonically toward the bottom, where they reach −0.4°C and −1.1°C at $M_{740}$ and $M_{530}$, respectively. The highest temperatures (above 0.7°C) are found toward the end of the records (Darelius et al., 2023).

The time-averaged current profiles (Figures 4a–4c) are bottom-enhanced at both moorings. The mean velocity increases by about 50% over the bottom-most 200 m, that is, roughly over the depth of the layer that is influenced by mWDW. The temperature profiles (Figure 4b), on the other hand, show that the temperature at any given depth is higher on $M_{530}$ than at $M_{740}$. This means that warm, dense (see Section 2.3) mWDW shoals toward the shelf break. The upward-sloping isotherms are also apparent in the temperature sections from the deployment cruise (Figure 2a). The difference in isotherm depth between the two moorings, $\Delta$ITD (Equation 1), is hence on average positive. The distribution of $\Delta$ITD consistently shifts toward higher values (i.e., steeper isotherm slope) for higher temperatures (Figure 5a). For water warmer than 0°C the time-averaged $\Delta$ITD is above 150 m. This is consistent with a bottom-enhanced westward flow in thermal wind balance (for a quantitative analysis, see Section 3.2.3 and

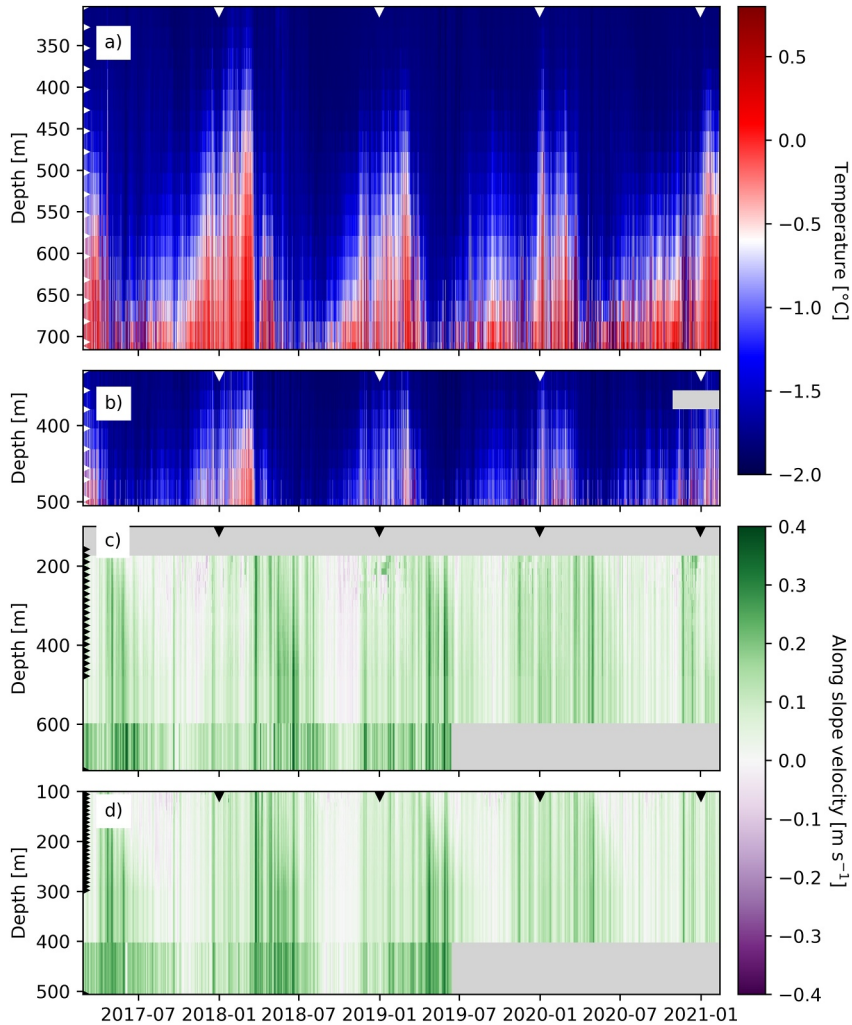


**Figure 3.** Hovmöller diagram of temperature at (a) $M_{740}$ and (b) $M_{530}$. Hovmöller diagram of alongslope velocity at (c) $M_{740}$ and (d) $M_{530}$. Triangles at the *y*-axis show the measurement depths, and the triangles on the upper *x*-axis mark 1 January of each year. The current meter data are low-pass filtered using a fifth-order Butterworth filter with a cut-off period of 48 hr to remove tides and topographic Rossby waves (Jensen et al., 2013). Note that the vertical scale differs between (a)–(b) and (c)–(d) and that the lower ADCP bin and point measurement of velocity are extended vertically over >100 m. Periods without data are marked in gray.

Figure 11). The velocity at the bottom at both $M_{740}$ and $M_{530}$ is higher for higher ΔITD (not shown), and the vertical velocity shear in the lower part of the water column is larger when the temperature at the bottom is high (Figure 5b).

### 3.2. Seasonal Variability

The seasonal variability in the region is, as elsewhere around the Antarctic margin, large. As summer transitions to winter, the daylight disappears, the temperature drops and the sea ice cover builds up and reaches close to 100% (Figure 6a). The seasonal freeze-melt cycle and a seasonally variable momentum transfer from the atmosphere induce seasonal changes in the upper ocean hydrography, which further affects the ASF/ASC system and modulates the inflow of mWDW onto the continental shelf east of Filchner Trough (Ryan et al., 2017; Årthun et al., 2012). While the local seasonal signal in the wind forcing is weak (Figure 6a), it has been shown that the ASC upstream of the study area is forced remotely (Lauber, Hattermann, et al., 2023; Le Paih et al., 2020). To describe the mean seasonality in the region, we use the 4 year-long time series to generate a seasonal climatology with monthly resolution.

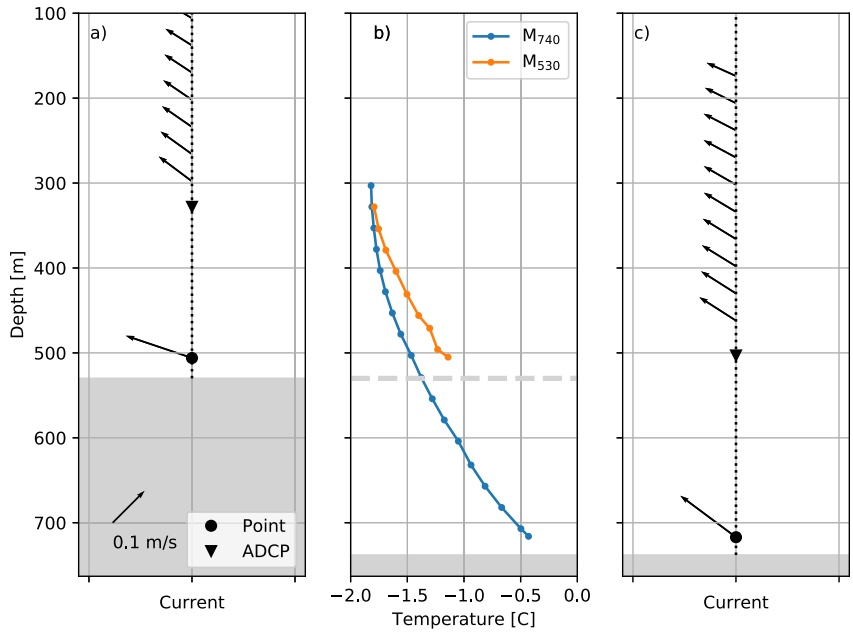


**Figure 4.** Time-averaged (a) current profile from $M_{530}$, (b) temperature profiles from $M_{740}$ and $M_{530}$ according to the legend and (c) current profile for $M_{740}$. The bottom depth is indicated in gray, where the dashed gray line in (b) is the bottom depth at $M_{530}$ and the filled box the bottom depth at $M_{740}$. The scale arrow in the lower left corner of (a) is valid for (a) and (c), and the velocity vectors shown are horizontal velocities. For clarity, results from every other (every fourth) ADCP-bin are shown in a(c).

### 3.2.1. Hydrography and Thermocline Depth

The temperature climatology confirms the seasonal change in thermocline depth above the continental slope apparent in Figures 3a and 3b and described by, for example, Semper and Darelius (2017). The mean position of the thermocline at $M_{740}$ is about 200 m shallower during austral summer than during winter (Figure 6b). The seasonality in thermocline depth is asymmetric, with a relatively abrupt drop in March-April (most clearly seen in Figure 3a, as interannual variability in the timing of the temperature drop smears the signal out in Figures 6b-c) and a more progressive shoaling during winter and spring. The mean bottom temperature is highest toward the end

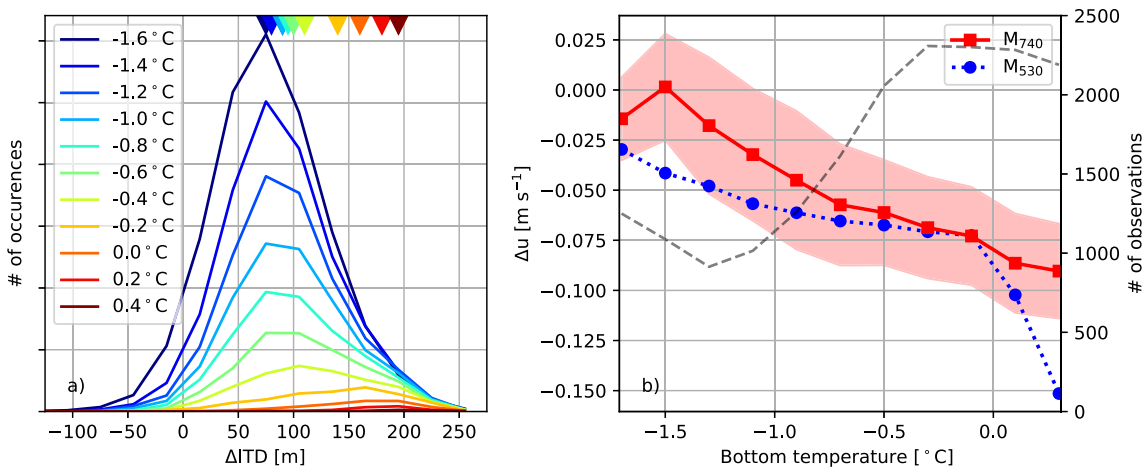


**Figure 5.** (a) Line histograms of ΔITD for isotherms according to the legend. The colored triangles at the upper *x*-axis show the time-averaged value of ΔITD for the respective isotherm. Positive values indicate that the isotherm is higher up in the water column on $M_{530}$ than on $M_{740}$. (b) Time-averaged difference in along slope velocity ($\Delta u$) between the two lowest levels with current measurements (see Table 1) in 0.2°C wide temperature bins for $M_{740}$ (red squares) and $M_{530}$ (blue circles). Negative values indicate that the velocity decreases upward. The shading shows a conservative estimate of the standard error (see Section 2.1) for $\Delta u$ (for $M_{740}$), and the dashed line shows the number of observations within each bottom temperature bin for $M_{740}$.

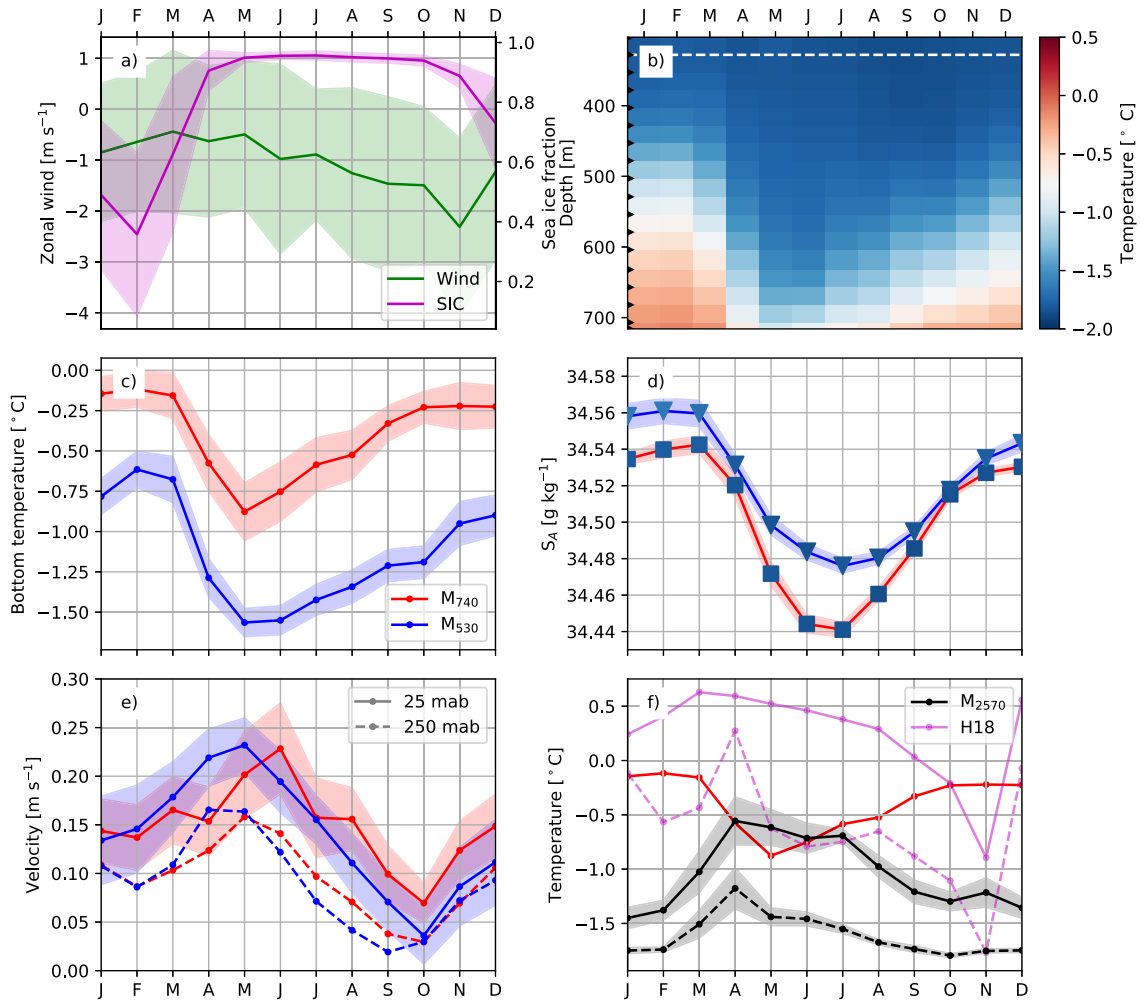


**Figure 6.** Mean seasonal cycle of (a) local zonal wind and sea ice concentration, (b) temperature as a function of depth at $M_{740}$, (c) bottom temperature (d) upper-level Absolute Salinity at $M_{740}$ (328 m, squares/red line, dashed white line in panel (b) and $M_{530}$ (354 m, triangles/blue line), (e) along-slope velocity, and (f) temperature at mooring $M_{2570}$ at 571 m (black line) and 371 m (dashed, black line) depth. The mean seasonal cycle in bottom temperature at $M_{740}$ (red line, from panel c) and the seasonal cycle extracted from the Kapp Norwegian climatology (marked H18 in the legend, Hattermann, 2018) at similar isobath and depths are included for comparison (magenta lines). In (b), the black triangles on the *y*-axis show the depth of the sensors, and in (a, c-f), the shaded area shows the standard error. The color of the markers in panel (d) shows the temperature at the same depth using the color scale from panel (b).

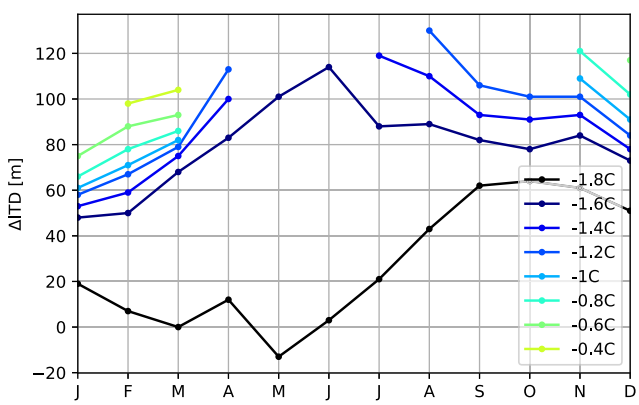


**Figure 7.** Monthly mean ΔITD for isotherms according to the legend. Only values for months when the isotherm was within the vertical range of the two moorings more than 25% of the time are shown.

of austral summer when it reaches close to 0°C at $M_{740}$. It is, on average, about 1°C lower during winter (Figures 6b and 6c). The mean difference in the depth of an isotherm between the moorings (ΔITD) was shown above to increase with increasing temperature. This pattern is also present when the analysis is carried out month by month, but, in addition, a seasonality of ΔITD is revealed (Figure 7). For all but the coldest isotherm (−1.8°C), ΔITD reaches a maximum during the winter months.

The hydrographic changes in the lower part of the water column follow the mixing line between WDW and WW (Figure 2b, triangles). This suggests that the variability results from the heaving and sinking of the WDW-WW interface and not from, for example, advection of a different water mass along the slope. Higher up (above 400 m) in the water column, the temperature remains at or close to the surface freezing point (−1.9°C) throughout the year, while the salinity varies. The Absolute Salinity at $M_{740}$, 328 m depth, is about 0.1 g kg$^{-1}$ higher during summer than in winter (Figure 2b, squares, and

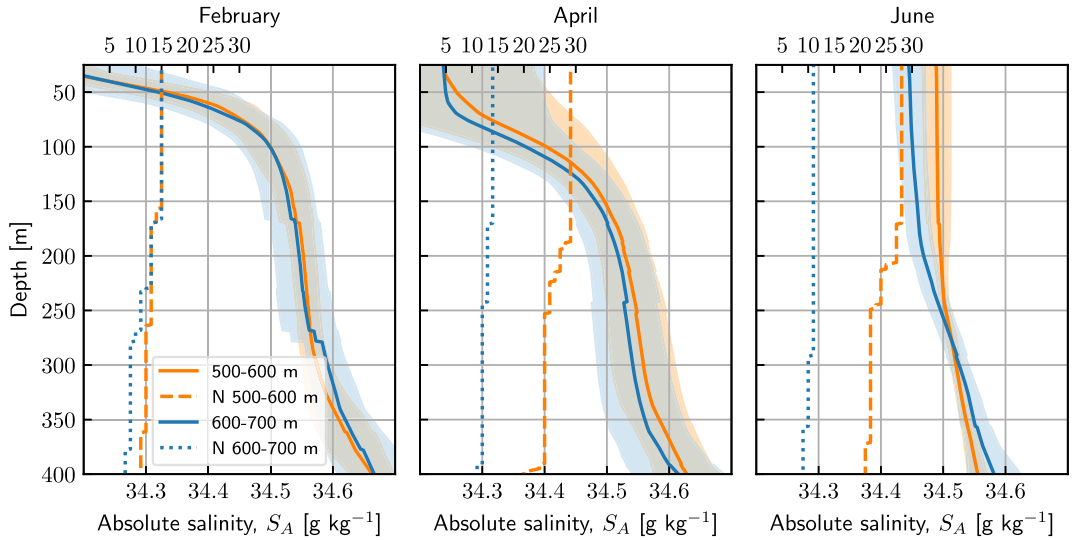


**Figure 8.** Monthly mean profiles of Absolute Salinity (continuous lines) collected by instrumented Weddell Seals between the 500–600 m isobath (orange) and the 600–700 m isobath (blue) in the shelf break region upstream of Filchner Trough. The standard deviation is given by color shading, and the number of profiles included in the mean profiles is indicated by the dashed lines following the upper horizontal axis. Only profiles with a thick (>150 m) WW layer ($\Theta < -1.8$°C) are included.

6 days). At $M_{530}$ (354 m depth), the phasing of the seasonality in salinity is similar, but since the amplitude is slightly lower, the difference in salinity between the two moorings is largest during winter (JJA) and smallest in autumn and spring. CTD profiles collected by instrumented Weddell Seals confirm the wintertime maximum in the salinity gradient between the two mooring locations and show that the signal extends up to the surface (Figure 8).

Interestingly, the seasonal signal in temperature observed at $M_{2570}$, located 80 km to the northeast of $M_{740}$, above the 2570 m isobath, is out of phase with the observations from $M_{740}$ and $M_{530}$; when the temperature drops above the upper part of the continental slope as the mWDW deepens, the temperature at $M_{2570}$ increases, suggesting that the mWDW *rises* above the deeper part of the slope (Figure 6f). A similar temperature maximum in March-April is observed at similar depths in the monthly climatology from Kapp Norwegian (Hattermann, 2018) above the deeper part of the slope (Figure 6f). However, these records all show an additional secondary temperature maximum in December-January. Lauber et al. (2024) (show similar out-of-phase behavior in thermocline depth between shallow and deep isobaths just east of the Fimbul Ice Shelf near the Prime Meridian.

### 3.2.2. Along-Slope Current

The seasonal changes in hydrography are accompanied by seasonality in the strength of the along-slope current. The current is strongest (0.20–0.25 m s$^{-1}$) at the bottom of $M_{740}$ and $M_{530}$ in autumn and weakest (<0.10 m s$^{-1}$) in spring (Figure 6e). Generally, the current above the upper slope increases when the thermocline deepens and the temperatures above the slope decrease (February-May, Figures 6b,c and e). This is consistent with a barotropic, along-slope current driven by Ekman convergence along the coast in the eastern part of the Weddell gyre (Le Paih et al., 2020). As surface water piles up along the coast, the barotropic current strengthens, and the thermocline depth increases.

The co-occurrence of weak currents and high temperatures is also apparent in the seasonal anomalies. When we subtract the mean seasonal signal (at monthly resolution, Figure 6) from records of monthly mean temperature and along-slope velocity, Figure 9, a consistent pattern appears; temperatures are generally above average for the first and last part of the record and below average in the middle part of the record. The along-slope velocity shows the opposite pattern, with velocities less than average in the first and last parts of the record. Over the full record, temperature and current anomalies are negatively correlated (typically $r \simeq -0.5$ at mid-level on $M_{740}$, significant at 95% level following Sciremammano (1979)) with the maximum correlation occurring at one month lag (current leads). The correlation is lower (typically $r \simeq -0.4$ and barely significant at 95%-level) at $M_{530}$.

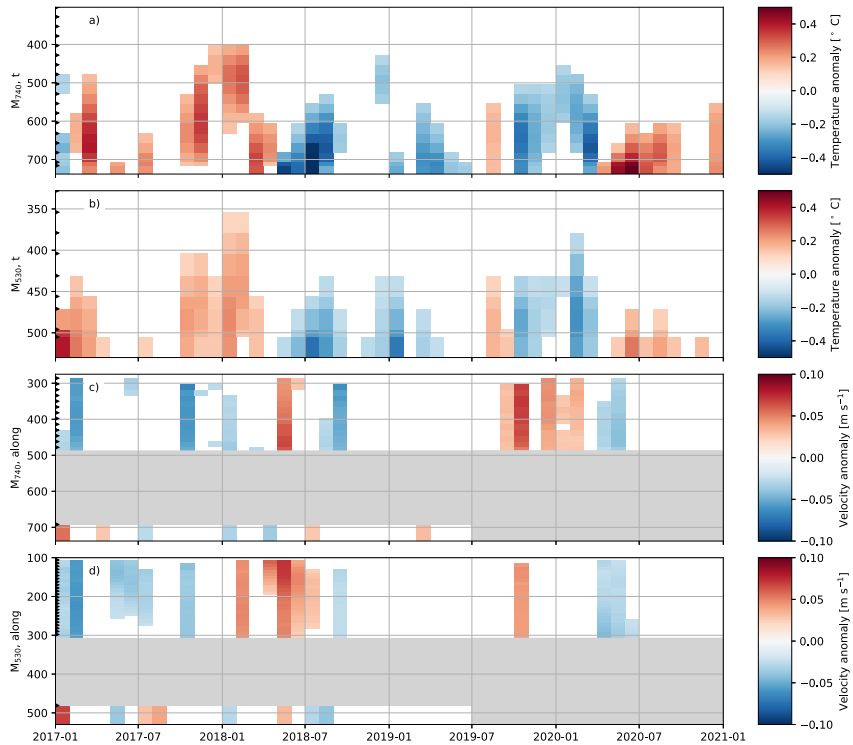


**Figure 9.** De-seasoned, monthly mean anomalies of temperature at (a) $M_{740}$ and (b) $M_{530}$ and of along slope velocity at (c) $M_{740}$ and (d) $M_{530}$. For clarity, only levels and months where the anomaly is larger than one standard deviation are shown, and the depth ranges without velocity measurements are colored gray. Note that the current meters at 25 mab stopped recording in June 2019 on both moorings.

### 3.2.3. Vertical Structure of the Current

Returning to the current measurements from $M_{530}$ and $M_{740}$, we note that it is not only the strength but also the vertical structure of the current that changes throughout the year (Figure 10). The vertical shear in the shallower part of the records (above 200 mab and typically within the WW-layer) and that of the lower part of the water column (affected by mWDW) evolves differently throughout the year. To highlight the difference in the seasonal evolution of the vertical shear, we show the monthly mean "bulk" gradient, $\Delta u/\Delta z$ of the two layers in Figure 11 and compare the results to the observed horizontal density gradients (using the equations for thermal wind balance) and seasonal changes in ΔITD (Figure 7) presented above. The currents above 200 mab show little change with depth during most of the year (August - March/April), while the vertical velocity gradients are relatively large during the winter months. The currents then increase with depth throughout most of the (observed) water column. The thermal wind balance implies that the density should increase toward the south during winter. Indeed, this is what is observed both at the moorings (Figures 6d and 11c) and in the CTD profiles collected by Weddell Seals (Figure 8). The observed shear (above 200 mab) is largest at $M_{530}$, but this is partly an artifact of the analysis, as the small depth range with data return during austral summer at $M_{740}$ limits the depth range over which the velocity gradient in Figure 11a is calculated. The vertical gradients are weaker and close to zero during spring and summer, especially at $M_{530}$. The magnitude of the vertical gradient over the upper layer agrees with thermal wind estimates using the observed horizontal density gradient (Figures 11a–11c).

We saw above (Figure 5) that the bottom enhancement is–at least partly–associated with high temperatures and mWDW "climbing" up along the bottom (i.e., upward-sloping isotherms). As bottom temperatures are higher during summer (Figure 6c), we would expect a seasonal signal in the bottom enhancement, that is, that the vertical velocity shear over the lower part of the water column would be largest during summer. This is, however, not observed (Figure 11b), potentially as the temperature effect is offset by the tendency for higher ΔITD (for a given isotherm) during winter (Figure 7).

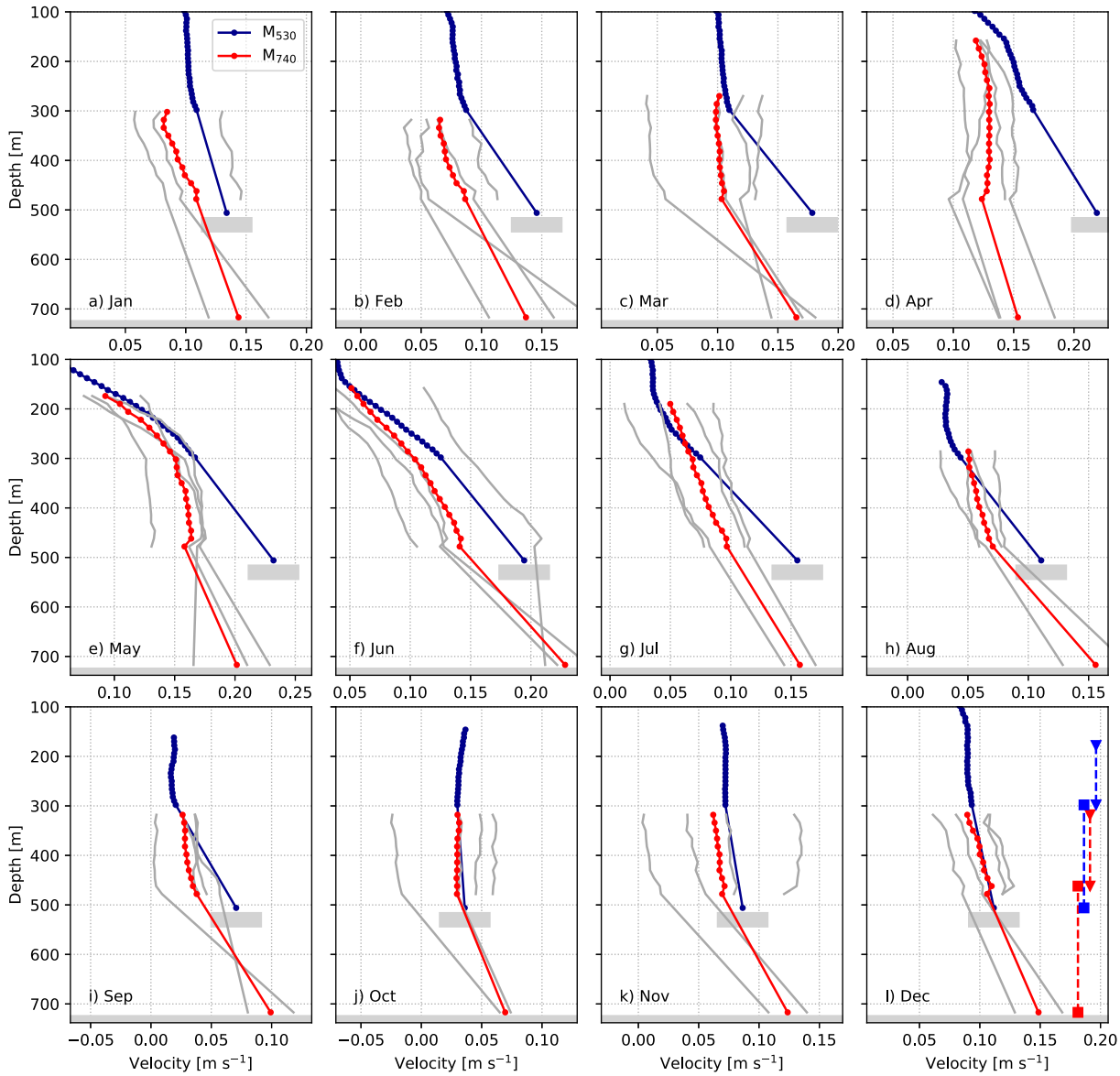


**Figure 10.** Deployment mean vertical profiles of along-slope velocity for (a) January, (b) February, (c) March, (d) April, (e) May, (f) June, (g) July, (h) August, (i) September, (j) October, (k) November and (l) December at $M_{740}$ (red) and $M_{530}$ (blue). Monthly mean profiles from individual years at $M_{740}$ are shown in gray. The velocity scale is centered around the value observed at $M_{740}$, 300 m depth, but the range shown is the same in all panels so that gradients are comparable. The dashed lines in (l) show the vertical range of $\Delta u$ shown in Figure 11.

## 4. Discussion

New observations spanning the period 2017–2021 from two moorings on the upper continental slope just east of the Filchner Trough reveal details of the structure, seasonality, and interannual variability (Darelius et al., 2023) of the southern part of the ASC/ASF in the southeastern Weddell Sea The study area is on the border between the "fresh shelf/surface-intensified ASC" in the east and the "dense shelf/bottom-intensified ASC" further west (Huneke et al., 2022; Thompson et al., 2018). The westward flowing current is bottom-enhanced, in agreement with the model results by Huneke et al. (2022), but contrary to their findings, the observations indicate strong seasonality also at depth; with strongest mean flow during April-June of 0.25 m $s^{-1}$ at 25 mab and 0.15 m $s^{-1}$ at 250 mab.

The vertical shear in the upper water column is largest when the current is strongest in April-June (Figure 10). This is due to an on-shore directed salinity gradient in the upper layer. The monthly mean along-slope velocities in April-June are 0.1–0.2 m $s^{-1}$ larger than the minimum velocities recorded in September-October. The seasonality

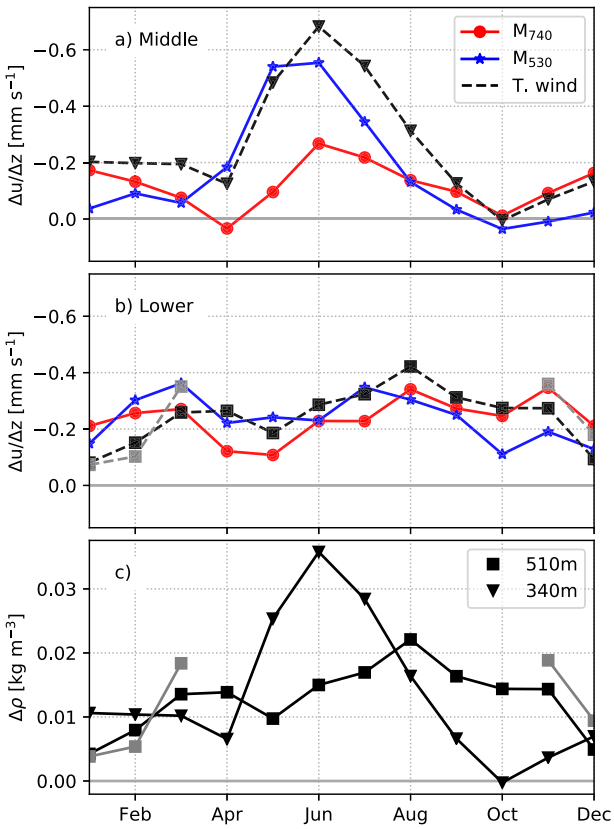


**Figure 11.** Monthly mean vertical gradients in the along slope velocity over (a) the middle and (b) the lower part of the water column. The dashed lines show the vertical velocity gradient estimated from the horizontal density difference between the two moorings (thermal wind) with density calculated from the observed temperature and salinity (black) and temperature only using Equation 2 (gray). Only months for which the temperature is within the temperature range for which Equation 2 is valid ($-1.5 < \Theta < 0.4$°C) at both moorings more than 75% of the time are shown. The depth ranges used for the different layers and moorings are indicated in Figure 10l. Note that the *y*-axis is reversed. Negative values indicate that the velocity increases toward the bottom. (c) Monthly mean in situ density difference between $M_{740}$ and $M_{530}$ at about 510 m (squares) and 340 m (triangles) depth calculated from observed salinity and temperature (black) and temperature only (gray). Positive values indicate that the density at $M_{530}$ is higher. Note that there is a ≃30 m difference in the depth of the conductivity sensors at the two moorings. The figure is based on data recorded before June 2019, that is, before the lower current meters stopped recording.

in the along-slope current is larger at the bottom than higher up in the water column and larger over shallower isobaths ($M_{530}$) than over deeper isobaths ($M_{740}$). The timing of the maximum velocities in late autumn observed at $M_{530}$ and $M_{740}$ aligns with maximum ASC transport inferred at 17°W (Graham et al., 2013) and with maximum velocities reported from the Prime Meridian and Kapp Norwegian (0/12°W, (Le Paih et al., 2020). We note, however, that the seasonal amplitude in $M_{530}$ and $M_{740}$ is larger by a factor of at least two compared to results reported by Le Paih et al. (2020, mooring data) and Auger et al. (2022 satellite data). This is potentially linked to the location above the slope, as the seasonality has been shown elsewhere to vary across the isobaths (Auger et al., 2022; Lauber et al., 2023).

The thermocline depth shows a pronounced seasonal cycle (Semper & Darelius, 2017; Årthun et al., 2012), with a vertical excursion of about 200 m in its (monthly) mean position. This vertical excursion in the monthly averaged records is distinct from excursions of similar amplitude on daily timescales caused by coastal trapped waves (Jensen et al., 2013). The thermocline is at its shallowest toward the end of the summer (February), and it then drops rapidly in Autumn (March-April) when the mWDW more or less completely disappears from $M_{530}$.

The seasonal inflow of mWDW onto the continental shelf east of Filchner Trough (Ryan et al., 2017; Årthun et al., 2012) occasionally reaches the Filchner Ice Shelf front (Darelius et al., 2016), and it is tightly linked to the seasonality above the slope. The thermocline deepens in March-April and shuts off the warm inflow, as mWDW is no longer available at depths shallower than the depth of the shelf break (Ryan et al., 2017). The prolonged warm inflow in 2017 (Ryan et al., 2020), during which warmer than usual mWDW was observed at oceanographic moorings on the shelf (CS, see Figure 1) several months longer than in the rest of the record (Ryan et al., 2017), does, however, not seem to be caused by a prolonged warm situation on the shelf break. While water during the inflow season of 2017 is warmer than "normal" (Figure 9), the warm water disappears from the upper part of the slope in April "as usual" (Figure 3b) and winter temperatures in 2017 at $M_{530/740}$ were not anomalously high.

We note that the period during which actual inflow, that is, southward flow, is observed at 76°S (Ryan et al., 2017, their "Phase 2" (roughly April-June), see their Figure 3) coincides with the period of maximum current strength at $M_{530}$ and $M_{750}$ (Figure 6e). The advection time scale from the shelf break to 76 S is on the order of several weeks or months, and since the mWDW appears at the 76 S mooring sites before or immediately after the currents here shift to a southward direction, there must have been southward flow on the continental shelf further north earlier in the season. One plausible explanation, consistent with the observations, is that a circulation cell on the shelf east of Filchner Trough, which includes a southward flow (of mWDW, when present) and a northward return flow above the eastern flank of Filchner Trough, extends further south in the period when the current over the shelf break is strongest.

### 4.1. The Upward Sloping Isotherms

Easterly winds and converging Ekman transports along the coast generally cause a southward deepening of the thermocline (Sverdrup, 1953), but the mooring records show a persistent upward slope of isotherms (and hence isopycnals) toward the shelf break. The upward slope of the isopycnals indicates a horizontal gradient in density with density decreasing off-shelf. Thermal wind balance then causes the westward current to increase toward the bottom. The agreement between the observed vertical velocity shear and the horizontal density gradient (Figures 11a and 11b) suggests that the thermal wind balance holds and that the flow is in approximately

geostrophic balance. This is expected, as we estimate the temporal Rossby number $\mathrm{Ro_T} = 1/\mathrm{f\,T} \simeq 0.1$, the Rossby number $\mathrm{Ro} = U/Lf \simeq 0.1$ and the Ekman number $\mathrm{Ek} = A_z/fH^2 \simeq 0.01$. Here $f = 10^{-4}$ s$^{-1}$ is the Coriolis factor, $A_z = 10^{-2}$ m$^2$ s$^{-1}$ the eddy viscosity and $T = 1$ day, $U = 0.1$ m s$^{-1}$, $L = 10$ km and $H = 100$ m are time, velocity, length and depth scales relevant for the flow. $L$ is chosen based on the discussion below and the distance to the "corner" of Filchner Trough, where the current is expected to be deflected southward.

Isotherms sloping upwards toward the shelf break are regularly observed above the continental slope in CTD sections from the southeastern Weddell Sea (Chavanne et al., 2010; Heywood et al., 1998; Nøst et al., 2011, and Figure 2). The uplift could potentially facilitate the on-shelf flow of warm water as mWDW is lifted to shallower depths - but the uplift is largest during winter when the warm inflow is limited (Figure 7). Nøst et al. (2011) suggest that one potential explanation for the shoaling isotherms (isopycnals) is the interaction between eddies and a sloping topography (Greatbatch & Li, 2000). We note, however, that the Eddy Kinetic Energy (EKE) in the region shows a pronounced maximum during summer (Darelius et al., 2023, their Figure 6), whereas the uplift (for a given isotherm) is largest during winter.

It is also possible that the presence of Filchner Trough is causing or contributing to the southward thermocline shoaling, as water columns are steered onto shallower isobaths to conserve potential vorticity when encountering the "corner" (i.e., the southward bending isobaths) of the Filchner Trough opening (Williams et al., 2001). To further investigate this effect, we apply the scaling for the radius of curvature, $R_c$, suggested by Williams et al. (2001) to a barotropic shelf break jet over a sloping bottom that encounters a sharp corner:

$$R_c = 1.3\sqrt{\frac{Uh_0}{f\nabla h}} \tag{3}$$

where $h_0$ the initial depth of the streamline considered, and the bottom slope $\nabla h \simeq 0.04$ at the mooring site (estimated from the difference in depth and distance between $\mathrm{M_{530}}$ and $\mathrm{M_{740}}$). If the horizontal shear of the jet is small compared to $f$ and we assume that changes in the shape of the jet as it moves around the corner can be ignored (in Williams et al. (2001) simulations, this largely holds above the slope but not on the shelf), then conservation of potential vorticity gives

$$\frac{f}{h_0} = \frac{f - U/R_c}{h_0 - \Delta h} \tag{4}$$

and we can solve for $\Delta h = F(U, \nabla h, h_0)$, where $\Delta$h is the change in depth of a water column needed to compensate for the change in potential vorticity of the turning jet. The value of $\Delta h$ increases for increasing values of $U$, $h_0$, and $\nabla h$ (Figure 12a) and are on the order of 100–200 m for values relevant to our mooring site. If the depth of a given isotherm upstream of the corner is $D_0$, then its relative depth ($D_0/h_0$) will be conserved as the jet moves onto shallower isobaths when approaching the corner, so that its depth at the corner $D_0'$ is given by

$$D_0' = \frac{D_0}{h_0}(h_0 - \Delta h). \tag{5}$$

The difference between $D_0$ and $D_0'$ is larger over shallower isobaths, and this gives rise to upward-sloping isotherms (Figure 12b). The scaling suggests that the effect could be noticeable at the mooring site and that it, in accordance with the observations, would increase with increasing velocities. Note, however, that realistic values for $U$ and $h_0$ give $R_c$ on the order of 10 km, while the distance between the moorings and the sharp bend in the 500 m isobath at the opening of Filchner Trough (see Figure 1) is twice or three times larger. In addition, the results and the scaling by Williams et al. (2001) are valid for a barotropic jet and a case where all isobaths make a corner, whereas, on the mooring site, the current has a baroclinic component (Figure 10) and only the shallower isobaths turn into Filchner Trough. A similar behavior, with streamlines "cutting the corner" to conserve potential vorticity, is, however, observed also in Williams et al. (2001)'s trough simulations, which largely resembles the setting at the Filchner Trough (albeit barotropic and in the northern hemisphere). It is not clear how stratification and the baroclinic component of the flow would affect the results.

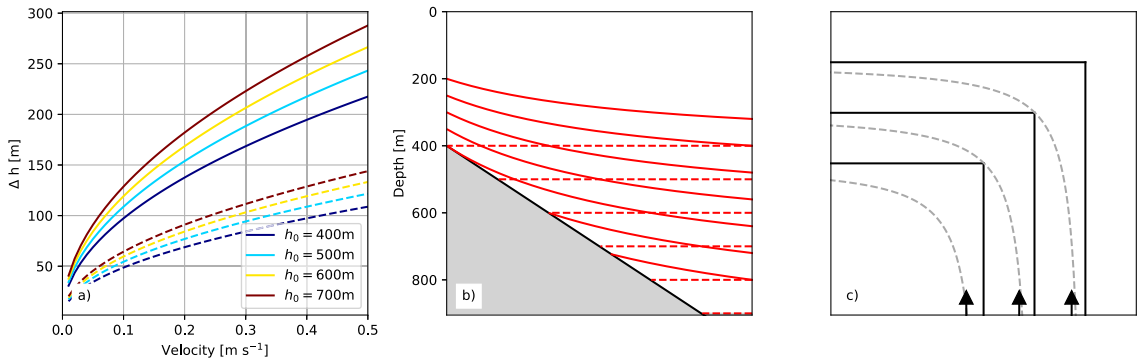


**Figure 12.** (a) Change in depth ($\Delta h$) for the turning jet as a function of velocity, for different initial depth of the streamlines ($h_0$, color according to legend) and slope ($\nabla h = 0.04$ solid lines and $\nabla h = 0.01$ dashed lines). (b) Position of (initially horizontal) isotherms after a $\Delta h = 200$ m onshore shift. (c) Sketch showing the streamlines (dashed lines) of a barotropic jet encountering a corner in the bathymetry (black lines) in the southern hemisphere. The current enters from the lower bottom (black arrows) and deeper water is to the right of the current (freely after Williams et al., 2001, their Figure 5).

## 5. Summary

We have analyzed the mean properties and the seasonal signal of the ASC/ASF system above the upper continental slope just east of the Filchner Trough based on new, four year-long mooring records. The structure of the ASC and the ASF in this region was previously undescribed, although it controls the access of warm water to the Filchner Trough and toward the Filchner Ice Shelf. Here we fill this gap, by providing a detailed description of the local ASF/ASC system and its variability. Our observations show that the ASC close to the shelf break has a mean strength of about 0.1 m s$^{-1}$, and that the current is bottom-enhanced. The vertical shear in the upper part of the water column is largest during austral winter when the horizontal salinity gradient between the relatively dense shelf and the fresher waters of the ASC is largest. The isotherms in the lower part of the water column shoal toward the shelf break, and since the isotherms are parallel to isopycnals, the tilt contributes to the bottom enhancement of the current. Maximum isotherm tilt is observed during winter, and it is larger for higher temperatures and stronger currents. We suggest that the shoaling is linked to local topography and the conservation of potential vorticity. As the ASC encounters the southward turning isobaths marking the opening of Filchner Trough, it climbs higher up on the slope to compensate for the potential vorticity induced by the curved streamlines.

The mooring records reveal a strong seasonality in the ASC/ASF system, with the highest along-slope velocities in April-June and the highest temperatures/shallowest thermocline in February-March. Anomalously strong currents appear to be connected to negative temperature anomalies at one month lag.

We provide the first description of the ASC/ASF system, its structure and variability in the climatically important region upstream of the Filchner Trough. Our description can serve as a benchmark for for example, numerical model simulation of the region and contribute to the dynamical understanding of shelf break processes and the propagation of anomalies along the southern rim of the Weddell Sea. Further observational and modeling studies are needed to understand the link between atmospheric forcing, the strength of the ASC/ASF and the inflow of warm water toward the ice shelf cavities.

## Data Availability Statement

Mooring data are available to download from Pangaea at https://doi.pangaea.de/10.1594/PANGAEA.964715 (M6 Darelius et al., 2024), https://doi.org/10.1594/PANGAEA.962043 (M3, 2017–2021, Darelius, 2023) and https://doi.org/10.1594/PANGAEA.869799 (M3, 2009–2010, Fer, 2016).

CTD-data are available from Pangaea athttps://doi.org/10.1594/PANGAEA.957614 (2021, Tippenhauer et al., 2023), from Seanoe at http://www.seanoe.org/data/00429/54012/ (2017, Sallée, 2018) and from MEOP (seal data, www.meop.net).

**Acknowledgments**
This work was funded by the Norwegian Research Council, projects 267660, 328941, and 295075. The moorings were recovered during the COSMUS expedition (PS124). NS received funding from the European Union's Horizon 2020 research and innovation program under grant agreement N°821001 (SO-CHIC). This research was supported by OCEAN:ICE, which is co-funded by the European Union, Horizon Europe Funding Programme for research and innovation under grant agreement Nr 101060452 and by UK Research and Innovation. This is O:I contribution number 10. ED is thankful to K. Makinson for the inspiring FRISP discussion about currents "cutting corners" many years ago.

## References

Årthun, M., Nicholls, K. W., Makinson, K., Fedak, M. A., & Boehme, L. (2012). Seasonal inflow of warm water onto the southern Weddell Sea continental shelf, Antarctica. *Geophysical Research Letters*, *39*(17), L17601. https://doi.org/10.1029/2012GL052856

Auger, M., Sallée, J. B., Prandi, P., & Naveira Garabato, A. C. (2022). Subpolar southern ocean seasonal variability of the geostrophic circulation from multi-mission satellite altimetry. *Journal of Geophysical Research: Oceans*, *127*(6). https://doi.org/10.1029/2021JC018096

Chavanne, C. P., Heywood, K. J., Nicholls, K. W., & Fer, I. (2010). Observations of the Antarctic slope undercurrent in the southeastern Weddell Sea. *Geophysical Research Letters*, *37*(13). https://doi.org/10.1029/2010GL043603

Daae, K., Hattermann, T., Darelius, E., & Fer, I. (2017). On the effect of topography and wind on warm water inflow - an idealized study of the southern Weddell Sea continental shelf system. *Journal of Geophysical Research: Oceans*, *122*(3), 2017–2033. https://doi.org/10.1002/2016JC012541

Daae, K., Hattermann, T., Darelius, E., Mueller, R. D., Naughten, K. A., Timmermann, R., & Hellmer, H. H. (2020). Necessary conditions for warm inflow towards the Filchner ice shelf, Weddell Sea. *Geophysical Research Letters*, *47*(22). https://doi.org/10.1029/2020GL089237

Darelius, E. (2023). Data processing: M3, southern Weddell Sea 2017-2021. *PANGAEA*. Retrieved from https://doi.pangaea.de/10.1594/PANGAEA.962043

Darelius, E., Dundas, V., Janout, M. A., & Tippenhauer, S. (2023). Sudden, local temperature increase above the continental slope in the Southern Weddell Sea, Antarctica. *Ocean Science*, *19*(3), 671–683. https://doi.org/10.5194/os-19-671-2023

Darelius, E., Fer, I., & Nicholls, K. W. (2016). Observed vulnerability of Filchner-Ronne Ice Shelf to wind-driven inflow of warm deep water. *Nature Communications*, *7*(1), 12300. https://doi.org/10.1038/ncomms12300

Darelius, E., Janout, M., Fer, I., & Sallée, J. B. (2024). Physical oceanography and current velocity data from mooring M6 on the upper continental slope, east of Filchner Trough, February 2017-2021. [Dataset]. https://doi.org/10.1594/PANGAEA.962043. *PANGAEA*

Darelius, E., Makinson, K., Daae, K., Fer, I., Holland, P. R., & Nicholls, K. W. (2014). Circulation and hydrography in the Filchner depression. *Journal of Geophyscial Research*, *119*, 1–18. https://doi.org/10.1002/2014JC010225

Emery, W. J., & Thomson, R. E. (2001). *Data analysis methods in physical oceanography - second and revised edition*. Elsevier.

Fahrbach, E., Rohardt, G., & Krause, G. (1992). The Antarctic coastal current in the southeastern Wedell sea. *Polar Biology*, *12*(2), 171–182. https://doi.org/10.1007/bf00238257

Fer, I. (2016). Moored measurements of current, temperature and salinity in the southern Weddell Sea, January 2009-January 2010. [Dataset]. https://doi.org/10.1594/PANGAEA.869799. *Berg: PANGAEA*

Foldvik, A., Gammelsrød, T., Østerhus, S., Fahrbach, E., Rohardt, G., Schröder, M., et al. (2004). Ice shelf water overflow and bottom water formation in the southern Weddell Sea. *Journal of Geophysical Research*, *109*(C2). https://doi.org/10.1029/2003JC002008

Foster, T. D., & Carmack, E. C. (1976). Frontal zone mixing and Antarctic bottom water formation in the southern Weddell Sea. *Deep-Sea Research*, *23*(4), 301–317. March 1975. https://doi.org/10.1016/0011-7471(76)90872-x

Fretwell, P., Pritchard, H. D., Vaughan, D. G., Bamber, J. L., Barrand, N. E., Bell, R., et al. (2013). Bedmap2: Improved ice bed, surface and thickness datasets for Antarctica. *The Cryosphere*, *7*(1), 375–393. https://doi.org/10.5194/tc-7-375-2013

Gill, A. E. (1973). Circulation and bottom water production in the Weddell Sea. *Deep-Sea Research*, *20*(2), 111–140. https://doi.org/10.1016/0011-7471(73)90048-x

Graham, J. A., Heywood, K. J., Chavanne, C. P., & Holland, P. R. (2013). Seasonal variability of water masses and transport on the Antarctic continental shelf and slope in the southeastern Weddell Sea. *Journal of Geophysical Research: Oceans*, *118*(4), 2201–2214. https://doi.org/10.1002/jgrc.20174

Greatbatch, R. J., & Li, G. (2000). Alongslope mean flow and an associated upslope bolus flux of tracer in a parameterization of mesoscale turbulance. *Deep-Sea Research Part I Oceanographic Research Papers*, *47*(4), 709–735. https://doi.org/10.1016/S0967-0637(99)00078-3

Hattermann, T. (2018). Antarctic thermocline dynamics along a narrow shelf with easterly winds. *Journal of Physical Oceanography*, *48*(10), 18–0064. https://doi.org/10.1175/JPO-D-18-0064.1

Hattermann, T., Smedsrud, L. H., Nøst, O. A., Lilly, J., & Galton-Fenzi, B. (2014). Eddy-resolving simulations of the Fimbul Ice Shelf cavity circulation: Basal melting and exchange with open ocean. *Ocean Modelling*, *82*, 28–44. https://doi.org/10.1016/j.ocemod.2014.07.004

Hellmer, H. H., & Holtappels, M. (2021). The expedition PS124 of the research vessel Polarstern to the southern Weddell Sea in 2021 (tech. Rep.). *Bremerhafen: Alfred Wegner Institute for Polar and Marine Research*. https://doi.org/10.48433/BzPM{_}0755{_}2021

Hellmer, H. H., Kauker, F., Timmermann, R., Determann, J., & Rae, J. (2012). Twenty-first-century warming of a large Antarctic ice-shelf cavity by a redirected coastal current. *Nature*, *485*(7397), 225–228. https://doi.org/10.1038/nature11064

Hellmer, H. H., Kauker, F., Timmermann, R., Hattermann, T., Shelf, F.-r. I., & Mengel, M. (2017). The fate of the southern Weddell Sea continental shelf in a warming climate. *Journal of Climate*, *30*(12), 4337–4350. https://doi.org/10.1175/JCLI-D-16-0420.1

Hersbach, H., Bell, B., Berrisford, P., Hirahara, S., Horányi, A., Muñoz-Sabater, J., et al. (2020). The ERA5 global reanalysis. *Quarterly Journal of the Royal Meteorological Society*, *146*(730), 1999–2049. https://doi.org/10.1002/qj.3803

Heywood, K. J., Locarnini, R. A., Frew, R. D., Dennis, P. F., & King, B. A. (1998). Transport and water masses of the Antarctic slope front system in the eastern Weddell Sea. In S. S. Jacobs & R. Weiss (Eds.), *Ocean, ice, and atmosphere - interaction at the Antarctic continental margin* (75th ed., Vol. 75, pp. 203–214). American Geophysical Union. https://doi.org/10.1029/AR075p0203

Heywood, K. J., Schmidtko, S., Heuzé, C., Kaiser, J., Jickells, T. D., Queste, B. Y., et al. (2014). Ocean processes at the Antarctic continental slope. *Philosophical Transactions of the Royal Society A: Mathematical, Physical & Engineering Sciences*, *372*(2019), 20130047. https://doi.org/10.1098/rsta.2013.0047

Hill, E. A., Rosier, S. H. R., Gudmundsson, G. H., & Collins, M. (2021). Quantifying the potential future contribution to global mean sea level from the Filchner-Ronne basin, Antarctica. *The Cryosphere Discussions*, 1–43. https://doi.org/10.5194/tc-2021-120

Huneke, W. G., Morrison, A. K., & Hogg, A. M. (2022). Spatial and sub-annual variability of the Antarctic slope current in an eddying ocean–sea ice model. *Journal of Physical Oceanography*, *52*(3), 347–361. https://doi.org/10.1175/JPO-D-21-0143.1

Jacobs, S. S. (1986). The Antarctic slope front. *Antarctic Journal of the United States*, *21*, 123–124.

Jensen, M. F., Fer, I., & Darelius, E. (2013). Low-frequency variability on the continental slope of the southern Weddell Sea. *Journal of Geophysical Research: Oceans*, *118*(9), 4256–4272. https://doi.org/10.1002/jgrc.20309

Lauber, J., de Steur, L., Hattermann, T., & Darelius, E. (2024). Observed Seasonal Evolution of the Antarctic Slope Current System off the Coast of Dronning Maud Land, East Antarctica. *Journal of Geophysical Research: Oceans*, *129*(4). Portico. https://doi.org/10.1029/2023jc020540

Lauber, J., Hattermann, T., de Steur, L., Darelius, E., Auger, M., Nøst, O. A., & Moholdt, G. (2023). Warming beneath an East Antarctic ice shelf due to increased subpolar westerlies and reduced sea ice. *Nature Geoscience*, *16*(October), 877–885. https://doi.org/10.1038/s41561-023-01273-5

Le Paih, N., Hattermann, T., Boebel, O., Kanzow, T., Lüpkes, C., Rohardt, G., et al. (2020). Coherent seasonal acceleration of the Weddell Sea boundary current system driven by upstream winds. *Journal of Geophysical Research: Oceans*, *125*(10), 1–20. https://doi.org/10.1029/2020JC016316

Nachtsheim, D. A., Ryan, S., Schröder, M., Jensen, L., Oosthuizen, W. C., Bester, M. N., et al. (2019). Foraging behavior of Weddell seals (Leptonychotes weddellii) in connection to oceanographic conditions in the southern Weddell Sea. *Progress in Oceanography*, *173*(April 2018), 165–179. https://doi.org/10.1016/j.pocean.2019.02.013

Naughten, K. A., De Rydt, J., Rosier, S. H., Jenkins, A., Holland, P. R., & Ridley, J. K. (2021). Two-timescale response of a large Antarctic ice shelf to climate change. *Nature Communications*, *12*(1), 1–10. https://doi.org/10.1038/s41467-021-22259-0

Nicholls, K. W., Boehme, L., Biuw, M., & Fedak, M. A. (2008). Wintertime ocean conditions over the southern Weddell Sea continental shelf, Antarctica. *Geophysical Research Letters*, *35*(21). https://doi.org/10.1029/2008GL035742

Nicholls, K. W., Østerhus, S., Makinson, K., Gammelsrød, T., & Fahrbach, E. (2009). Ice-Ocean processes over the continental shelf of the southern Weddell Sea, Antarctica: A review. *Reviews of Geophysics*, *47*(3), 1–23. https://doi.org/10.1029/2007RG000250

Nissen, C., Timmermann, R., Hoppema, M., Gürses, O., & Hauck, J. (2022). Abruptly attenuated carbon sequestration with Weddell Sea dense waters by 2100. *Nature Communications*, *13*(1), 3402. https://doi.org/10.1038/s41467-022-30671-3

Nøst, O. A., Biuw, M., Tverberg, V., Lydersen, C., Hattermann, T., Zhou, Q., et al. (2011). Eddy overturning of the *Antarctic* slope front controls glacial melting in the eastern Weddell Sea. *Journal of Geophysical Research*, *116*(C11), C11014. https://doi.org/10.1029/2011JC006965

Nunez-Riboni, I., & Fahrbach, E. (2009). Seasonal variability of the Antarctic coastal current and its driving mechanisms in the Weddell Sea. *Deep Sea Research Part I: Oceanographic Research Papers*, *56*(11), 1927–1941. https://doi.org/10.1016/j.dsr.2009.06.005

Orsi, A. H., Smethie, W. M., & Bullister, J. L. (2002). On the total input of Antarctic waters to the deep ocean: A preliminary estimate from chlorofluorocarbon measurements. *Journal of Geophysical Research*, *107*(C8). https://doi.org/10.1029/2001JC000976

Pritchard, H. D., Ligtenberg, S. R. M., Fricker, H. A., Vaughan, D. G., Broeke, M. R. V. D., Padman, L., & van den Broeke, M. R. (2012). Antarctic ice-sheet loss driven by basal melting of ice shelves. *Nature*, *484*(7395), 502–505. https://doi.org/10.1038/nature10968

Rignot, E., Jacobs, S. S., Mouginot, J., & Scheuchl, B. (2013). Ice-shelf melting around Antarctica. *Science (New York, N.Y.)*, *341*(6143), 266–270. https://doi.org/10.1126/science.1235798

Ryan, S., Hattermann, T., Darelius, E., & Schröder, M. (2017). Seasonal cycle of hydrography on the eastern shelf of the Filchner Trough, Weddell Sea, Antarctica. *Journal Geophysical Research - Oceans*, *122*(8), 6437–6453. https://doi.org/10.1002/2017JC012916

Ryan, S., Hellmer, H. H., Janout, M., Darelius, E., Schröder, M., & Schröder, M. (2020). Exceptionally warm and prolonged flow of warm deep water toward the filchner-ronne ice shelf in 2017. *Geophysical Research Letters*, *47*(13), 1–24. https://doi.org/10.1029/2020GL088119

Sallée, J. B. (2017). WAPITI cruise, RV JAMES CLARK ROSS. *Technical Report D*. https://doi.org/10.17600/18002130

Sallée, J. B. (2018). Hydrological and current data for the Southern Weddell Sea, collected as part of the WAPITI oceanographic survey (JR16004). [Dataset]. *SEANOE*. https://doi.org/10.17882/54012

Sciremammano, F. J. (1979). A suggestion for the presentation of correlations and their significance levels. *Journal of Physical Oceanography*, *9*(6), 1273–1276. https://doi.org/10.1175/1520-0485(1979)009<1273:asftpo>2.0.co;2

Semper, S., & Darelius, E. (2017). Seasonal resonance of diurnal coastal trapped waves in the Weddell Sea, Antarctica. *Ocean Science*, *13*(1), 77–93. https://doi.org/10.5194/os-13-77-2017

Shepherd, A., Fricker, H. A., & Farrell, S. L. (2018). Trends and connections across the Antarctic cryosphere. *Nature*, *558*(7709), 223–232. https://doi.org/10.1038/s41586-018-0171-6

Smedsrud, L. H., Jenkins, A., Holland, D. M., & Nøst, O. A. (2006). Modeling ocean processes below Fimbulisen, Antarctica. *Journal of Geophysical Research*, *111*(C1), C01007. https://doi.org/10.1029/2005JC002915

Stewart, A. L., Klocker, A., & Menemenlis, D. (2019). Acceleration and overturning of the Antarctic slope current by winds, eddies, and tides. *Journal of Physical Oceanography*, *49*(8), 2043–2074. https://doi.org/10.1175/jpo-d-18-0221.1

Stewart, A. L., & Thompson, A. F. (2015). Eddy-mediated transport of warm circumpolar deep water across the Antarctic shelf break. *Geophysical Research Letters*, *42*(2), 432–440. https://doi.org/10.1002/2014GL062281.1

Stokes, C. R., Abram, N. J., Bentley, M. J., Edwards, T. L., England, M. H., Foppert, A., et al. (2022). Response of the east Antarctic ice sheet to past and future climate change. *Nature*, *608*(April 2021), 275–286. https://doi.org/10.1038/s41586-022-04946-0

Sverdrup, H. (1953). The currents off the coast of Queen Maud land. *Norsk Geografisk Tidskrift*, *14*(1), 239–249. https://doi.org/10.1080/00291955308542731

Thompson, A. F., Speer, K. G., & Schulze Chretien, L. M. (2020). Genesis of the Antarctic slope current in west Antarctica. *Geophysical Research Letters*, *47*(16). Retrieved from https://doi.org/10.1029/2020GL087802

Thompson, A. F., Stewart, A. L., Spence, P., & Heywood, K. J. (2018). The Antarctic slope current in a changing climate. *Reviews of Geophysics*, *56*(4), 741–770. Retrieved from https://doi.org/10.1029/2018RG000624

Tippenhauer, S., Janout, M. A., Schall, E., Timmermann, R., van Caspel, M., Vignes, L., et al. (2023). Physical oceanography based on ship CTD during POLARSTERN cruise PS124. [Dataset]. Retrieved from https://doi.org/10.1594/PANGAEA.957614

Treasure, A. M., Roquet, F., Ansorge, I. J., Bester, M. N., Boehme, L., Bornemann, H., et al. (2017). Marine mammals exploring the oceans pole to pole: A review of the MEOP consortium. *Oceanography*, *30*(2), 132–138. https://doi.org/10.5670/oceanog.2017.234

Whitworth, T., Orsi, A., Kim, S.-J., Nowlin, W. D., & Locarnini, R. A. (1998). Water masses and mixing near the Antarctic slope front. In S. S. Jacobs & R. F. Weiss (Eds.), *Ocean, ice, and atmosphere: Interactions at the Antarctic continental margin* (Vol. 75, pp. 1–27). American Geophysical Union. https://doi.org/10.1029/ar075p0001

Williams, W. J., Gawarkiewicz, G. G., & Beardsley, R. C. (2001). The adjustment of a shelfbreak jet to cross-shelf topography. *Deep-Sea Research Part II Topical Studies in Oceanography*, *48*(1–3), 373–393. https://doi.org/10.1016/S0967-0645(00)00085-0